(Received 27 March 2024, Accepted 19 May 2024, Scheduled 4 June 2024)

# Simplified Three-Vector Selection Model Predictive Current Control for PMSM Considering Fixed Switching Frequency

Dingdou Wen[1], Zhuoheng Li[1], Xiaorui Wei[1], and Zhun Cheng[2,*]

[1]*Hunan University of Technology, Zhuzhou 412007, China*
[2]*Hunan Railway Professional Technology College, Zhuzhou 412001, China*

**ABSTRACT:** To address the insufficiency of large computation and unfixed switching frequency in permanent magnet synchronous motor (PMSM) of three-vector model predictive current control (TV-MPCC), simplified three-vector selection model predictive current control (STV-MPCC) for PMSM considering fixed switching frequency is proposed. Firstly, a novel voltage vector selection strategy is constructed by calculating the reference voltage in combination with the deadbeat control and redividing the sectors, reducing the number of optimizations from 11 to 5. Then, the current error is introduced in the calculation of the duty cycle to simplify the conventional control algorithm. The current ripple is reduced, and the system switching frequency is fixed. Finally, the experimental results indicate that compared with the conventional TV-MPCC, the *d-q* axis current ripple has been reduced by 13% and 18%, respectively, and the torque ripple has been reduced by 6%, THD decreased from 4.70% to 4.25%, and the steady-state performance of the motor is improved.

## 1. INTRODUCTION

Due to the advantages of simple construction, reliable operation, high efficiency, and high power density, etc. permanent magnet synchronous motor (PMSM) has been widely used in high-performance speed control fields such as rail transportation, aerospace, and industrial drives [1–4].

Conventional PMSM control methods mainly include field-orientation control (FOC) and direct torque control (DTC). Among them, FOC relies on space vector pulse width modulation (SVPWM), resulting in slow system response speed, controller output lagging behind current changes, and poor dynamic response performance [5, 6], while DTC tends to use a single voltage vector action, resulting in large torque ripple and weak robustness [7].

Compared with FOC, the finite state set model predictive current control (FCS-MPCC) does not rely on SVPWM and directly outputs the inverter drive signal, which has a simple structure and better dynamic performance [8, 9]. However, it relies on the model parameters and is computationally intensive. In [10], a supertwisting-algorithm-based second-order sliding-mode observer is designed, but the observer design is complex and has high difficulty in parameter tuning. In [11], a model-free control method is proposed, which does not rely on motor model parameters and has good control effects. However, the controller design is complex, and robustness is poor. In [12], a sliding membrane observer is designed to improve the stability of the system against parameter perturbations to a certain extent, but its jitter and tracking errors are large. In [13], delay compensation and multi-step prediction algorithms are proposed to optimize the computational delay and improve the steady-state performance of the motor, but the computation is still large. In [14], the optimal voltage vector selection strategy is proposed, and the optimal voltage vector selection table is designed to simplify the algorithm, but the switching frequency is not fixed.

Due to the conventional single vector model predictive current control (SV-MPCC) outputting a single voltage vector in each control cycle, the optional voltage range is limited, which leads to a large current ripple and poor system steady-state performance. In [15], a dual-vector control strategy (DV-MPCC), which outputs an optimal voltage vector and a zero-vector duty cycle combination in one control cycle, can realize the output of an effective voltage vector with arbitrary amplitude. To achieve the output effective voltage vector with arbitrary direction and amplitude, in [16], a control strategy in which the second voltage vector is not fixed as a zero vector is proposed, and the second voltage vector is selected to consider the adjacent voltage vector, reducing the switching frequency. However, the voltage selection range of the DV-MPCC strategy is limited; the current ripple is large; and the switching frequency is high and not fixed. In [17], a three-vector model predictive current control (TV-MPCC) is proposed, which selects the third vector as the zero vector, resulting in a smaller current ripple and better steady-state performance. However, its first voltage vector needs to be predicted six times by the cost function, and the second voltage vector selection requires five times. The selection of optimal voltage vector is complex, computationally large, and demanding on hardware, which will affect the system control effect to some extent. In [18], a three-vector control strategy with fixed switching frequency is proposed to reduce and fix the switching frequency by utilizing a vector selection table combined with a three-stage modulation strategy. However, it relies on the cost function and does not consider

* Corresponding author: Zhun Cheng (120277982@qq.com).

current error in the duty cycle calculation. In [19], a voltage vector selection strategy is proposed, which combines the optimal voltage vector with five other sets of vectors and adds the zero vector to expand the voltage selection range. However, it is computationally complex and requires high system hardware. Therefore, while ensuring the excellent steady-state performance of model predictive control in the system, how to simplify the model prediction algorithm and fix the switching frequency has become a hot topic in model predictive control research [20–22].

To effectively simplify the conventional three-vector model prediction algorithm and fix the switching frequency, combined with deadbeat control, a simplified three-vector selection model predictive current control (STV-MPCC) for PMSM considering fixed switching frequency is proposed. The simplified voltage vector selection strategy is devised; the switching frequency of the inverter is fixed; and the current ripple is reduced. The main contributions of this paper are as follows:

(1) The proposed STV-MPCC designs a vector selection strategy that reduces the 11 predictions of conventional TV-MPCC algorithms to 5 by redefining sectors, and the system complexity has been reduced.

(2) The proposed method can select a combination of voltage vectors with a fixed switching frequency by employing seven levels of modulation in one control cycle to achieve fixed switching frequency control and reduce switching losses.

(3) STV-MPCC introduces current error in duty cycle calculation, and the current and torque ripple are effectively suppressed.

## 2. MATHEMATICAL MODEL OF PMSM

The $d$-$q$ coordinate system mathematical model of PMSM can be represented as [23].

$$\begin{cases} \frac{di_d}{dt} = \frac{1}{L_s}\left(u_d - R_s i_d + \omega_e L_q i_q\right) \\ \frac{di_q}{dt} = \frac{1}{L_s}\left(u_q - R_s i_q - \omega_e L_d i_d - \omega_e \psi_f\right) \end{cases} \tag{1}$$

where $i_d$, $i_q$, $u_d$, and $u_q$ are the $d$-$q$ axis stator currents and stator voltages, respectively; $L_d$ and $L_q$ are the $d$-$q$ axis stator inductances; $\omega_e$ is the electrical angular velocity; $R_s$ and $\psi_f$ are the stator resistance and permanent magnet magnetic linkage, respectively.

The expression of a first order forward Eulerian discretization of (1) is as follows:

$$\begin{cases} i_d(k+1) = i_d(k) + \frac{T_s}{L_d}\left(u_d(k) - R_s i_d(k) - e_d(k)\right) \\ i_q(k+1) = i_q(k) + \frac{T_s}{L_q}\left(u_q(k) - R_s i_q(k) - e_q(k)\right) \end{cases} \tag{2}$$

$$\begin{cases} e_d = -\omega_e L_q i_q \\ e_q = \omega_e\left(L_d i_d + \psi_f\right) \end{cases} \tag{3}$$

where $k$ is the current sampling time, $k+1$ the next sampling time, and $T_s$ the sampling period.

## 3. CONVENTIONAL TV-MPCC STRATEGY

In conventional TV-MPCC, it is necessary to rely on the cost function to optimize three of the eight basic voltage vectors in Fig. 1, calculate the action time of each voltage vector, and synthesize effective voltage vectors in any direction and amplitude based on this.

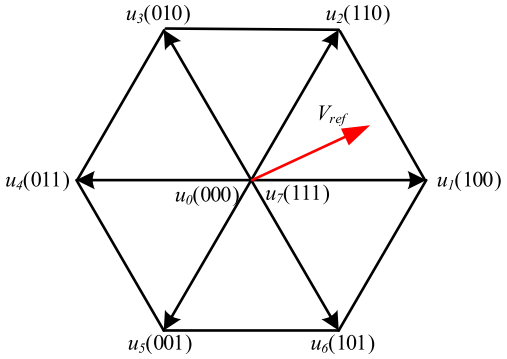


**FIGURE 1**. Basic voltage vector.

Substituting 6 basic effective voltage vectors into (2), 6 current predicted values are calculated. Compared with the current reference value, the predicted value is selected closest to the current reference value, and the selection of the optimal voltage vector is completed. Therefore, the cost function is often represented as:

$$g = \left(i_d^{ref} - i_d^{k+1}\right)^2 + \left(i_q^{ref} - i_q^{k+1}\right)^2 \tag{4}$$

where $i_d^{ref}$ and $i_q^{ref}$ are the $d$-$q$ axis reference currents, and $i_d^{k+1}$ and $i_q^{k+1}$ are the $d$-$q$ axis predicted currents, respectively. In the control strategy of $i_d^{ref} = 0$, $i_q^{ref}$ is output by the speed loop controller.

To calculate the duty cycle of each voltage vector, the $d$-$q$ axis predicted current can be represented by time and slope as:

$$\begin{cases} i_d(k+1) = i_d(k) + s_{xd}t_x + s_{yd}t_y + s_{zd}t_z \\ i_q(k+1) = i_q(k) + s_{xq}t_x + s_{yq}t_y + s_{zq}t_z \end{cases} \tag{5}$$

where $t_x$, $t_y$, and $t_z$ are the action times of the first, second, and third voltage vectors, respectively. $s_{xd}$, $s_{xq}$, $s_{yd}$, $s_{yq}$, $s_{zd}$, and $s_{zq}$ are the $d$-$q$ axis current slopes for the first, second, and zero vector actions, respectively.

By substituting the voltage vector selected through the value function into (5), the voltage slope can be calculated.

$$\begin{cases} s_{xd} = \frac{\mathrm{d}i_d}{\mathrm{d}t}\Big|_{u_d=u_{xd}} = \frac{1}{L_d}\left(-R_s i_d + \omega_r L_q i_q + u_{xd}\right) \\ s_{xq} = \frac{\mathrm{d}i_d}{\mathrm{d}t}\Big|_{u_q=u_{xq}} = \frac{1}{L_q}\left(-R_s i_q - \omega_r L_d i_d - \omega_r \varphi_f + u_{xq}\right) \end{cases} \tag{6}$$

$$\begin{cases} s_{yd} = \frac{\mathrm{d}i_d}{\mathrm{d}t}\Big|_{u_d=u_{yd}} = \frac{1}{L_d}\left(-R_s i_d + \omega_r L_q i_q + u_{yd}\right) \\ s_{yq} = \frac{\mathrm{d}i_d}{\mathrm{d}t}\Big|_{u_q=u_{yq}} = \frac{1}{L_q}\left(-R_s i_q - \omega_r L_d i_d - \omega_r \varphi_f + u_{yq}\right) \end{cases} \tag{7}$$

$$\begin{cases} s_{zd} = \frac{\mathrm{d}i_d}{\mathrm{d}t}\Big|_{u_d=u_{zd}} = \frac{1}{L_d}\left(-R_s i_d + \omega_r L_q i_q\right) \\ s_{zq} = \frac{\mathrm{d}i_d}{\mathrm{d}t}\Big|_{u_q=u_{zq}} = \frac{1}{L_q}\left(-R_s i_q - \omega_r L_d i_d - \omega_r \varphi_f\right) \end{cases} \tag{8}$$

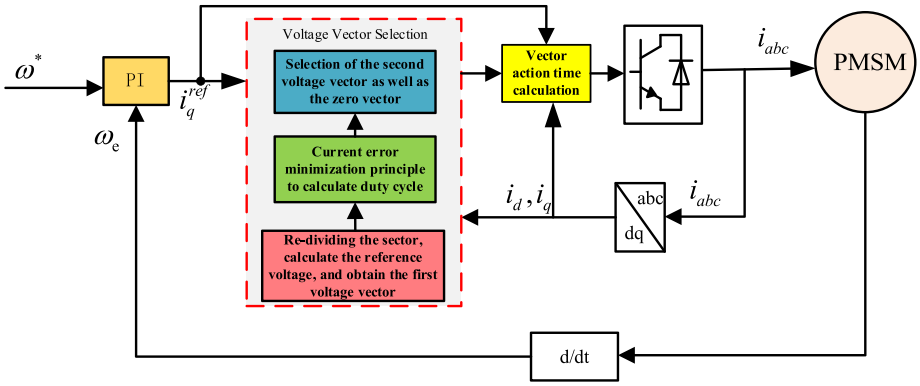


**FIGURE 2**. The control diagram of STV-MPCC.

where $u_x$, $u_y$, and $u_z$ are the $d$-$q$ axis components of the first, second, and third voltage vectors, respectively.

From (6), (7), and (8), the action times $t_x$, $t_y$, and $t_z$ of the three voltage vectors can be expressed as follows:

$$\begin{aligned} t_x &= 1/D[(i_d^* - i_d(k))((s_{zq} - s_{yq}) \\ &\quad +(i_q^* - i_q(k))(s_{yq} - s_{zq}) + T_S(s_{zd}s_{yq} - s_{yd}s_{zq})] \quad (9) \\ t_y &= 1/D[(i_d^* - i_d(k))((s_{xq} - s_{zq}) \\ &\quad +(i_q^* - i_q(k))(s_{zd} - s_{xd}) + T_S(s_{xd}s_{zq} - s_{sd}s_{xq})] \quad (10) \end{aligned}$$

where $D = s_{zd}s_{yq} - s_{zd}s_{xq} + s_{xd}s_{zq} - s_{yd}s_{zq} - s_{xd}s_{yq} + s_{yd}s_{xq}$.

The zero-vector action time is:

$$t_z = T_s - (t_x + t_y) \quad (11)$$

The implementation method of the conventional TV-MPCC strategy is as follows:

1) Six basic voltage vectors are introduced into (2) to predict the $d$-$q$ axis current six times.

2) Using the cost function to traverse the optimization process 6 times, the first and most significant voltage vector is selected, and repeat optimization in the remaining 5 basic voltage vectors. Then, select the third voltage vector from the two zero-vectors.

3) Combining (9), (10), and (11), the action time of each voltage vector is calculated by the slope of the current, and synthesize effective voltage vectors in any direction and angle.

## 4. SIMPLIFIED VECTOR SELECTION STRATEGY FOR STV-MPCC

The conventional TV-MPCC requires 11 times of cost function optimization, with complex calculations and irregular switching frequency variations, resulting in a significant burden on digital signal processors. To address the above deficiencies, a simplified vector selection strategy is proposed to output effective voltage vectors $u_1$, $u_2$, and $u_3$ with fixed switching frequency. As shown in Fig. 2, the control system diagram is shown.

To reduce system complexity, the deadbeat control method is adopted to calculate the reference voltage $V_{ref}$ for each cycle. According to the principle of deadbeat, it can be concluded that $i_d(k+1) = i_d^{ref}$, $i_q(k+1) = i_q^{ref}$.

From (2), reference voltage of $d$-$q$ axis can be obtained as follows:

$$\begin{cases} u_d^{ref} = R_s i_d(k) + \frac{L_d}{T_s}(i_d^{ref}(k+1) - i_d(k)) - \omega_e(k) L_q i_q \\ u_q^{ref} = R_s i_q(k) + \frac{L_q}{T_s}(i_q^{ref}(k+1) - i_q(k)) - \omega_e L_d i_d \\ \qquad +\psi_f \omega_e(k) \end{cases} \quad (12)$$

where $u_d^{ref}$, $u_q^{ref}$ are the components of the $d$-$q$-axis reference voltage; $i_d^{ref}$, $i_q^{ref}$ are the $d$-$q$-axis reference currents; $i_d(k)$, $i_q(k)$, and $\omega_e(k)$ are the $d$-$q$-axis currents and speed at moment $k$.

### 4.1. Selection of the First Voltage Vector

The conventional TV-MPCC performs six optimization searches through the cost function. However, STV-MPCC only requires one sector judgment to select the optimal first voltage vector from the three candidate first voltage vectors. Therefore, optimization can be achieved without relying on cost functions, reducing the complexity of the algorithm.

To simplify the selection of the optimal first voltage vector, the effective voltage vector is re-delineated into 3 sectors, as shown in Fig. 3.

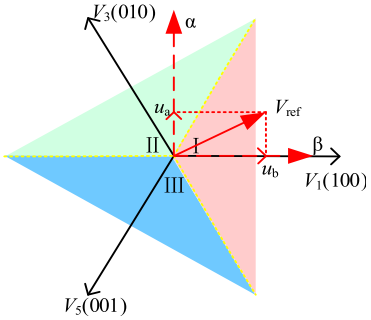


**FIGURE 3**. Re-dividing sectors.

To calculate which sector the reference voltage falls in, it is necessary to calculate the angle of the reference voltage. By performing the inverse park transformation on (12), the reference voltage in the $\alpha$-$\beta$ coordinate system can be represented

as

$$\begin{bmatrix} u_\alpha \\ u_\beta \end{bmatrix} = \begin{bmatrix} \cos\theta & -\sin\theta \\ \sin\theta & \cos\theta \end{bmatrix} \begin{bmatrix} u_d \\ u_q \end{bmatrix} \tag{13}$$

where $u_\alpha$ and $u_\beta$ denote the components of $V_{ref}$ in the $\alpha$-$\beta$ coordinate system, respectively, and $\theta$ is the electrical angle of the rotor.

Taking the phase angle of $u_\alpha$ and $u_\beta$ as the angle of the reference voltage in the $\alpha$-$\beta$ coordinate system, $\theta_{\alpha\beta}$ can be expressed as

$$\theta_{\alpha\beta} = \arctan\left(\frac{u_\alpha}{u_\beta}\right) \tag{14}$$

$$\text{sec} = floor\left[(\theta_{ab} + 30)/120 + 1\right] \tag{15}$$

where $\theta_{ab}$ is the phase angle; sec indicates the sector where the reference voltage resides; and the function *floor* denotes downward rounding.

For example, if sec $= 1$, the reference voltage $V_{ref}$ falls on the first sector in Fig. 4. Therefore, the optimal first voltage vector should be selected as $V_1$. Similarly, if sec $= 2$, the optimal first voltage vector should be chosen as $V_3$.

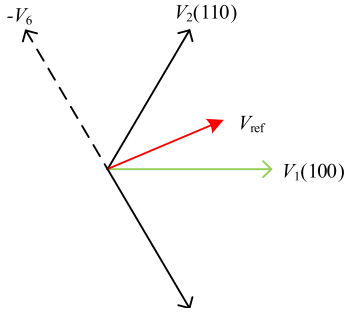


**FIGURE 4**. Second voltage vector selection.

### 4.2. Selection of the Second Voltage Vector

According to the first voltage vector selected, the second voltage vector is selected among its two neighbouring voltage vectors to minimize the number of switching actions.

As shown in Fig. 4, when the reference voltage falls on the first sector, the first voltage vector is selected as $V_1$. When the second voltage vector is selected adjacent to $V_1$ ($V_2$, $V_6$), the switch only needs to act once, i.e., the inverter is changed from the state (100) to the state (110) or (101), so that the second voltage vector is output at the minimum switching loss. Therefore, in the selection of the second voltage vector, only $V_2$ and $V_6$ are considered for the selected voltage vector.

To synthesize $V_{ref}$ in Fig. 4, one of $V_2$ or $V_6$ is required to act in conjunction with $V_1$. If $V_6$ is selected as the voltage vector to be selected, the duty cycle of $V_6$ is calculated to be negative, i.e., $-V_6$ and $V_1$ work together. If $V_2$ and $V_1$ are selected to act together, the duty cycle is positive. Because the negative duty cycle of the inverter output has no real physical meaning, the voltage vector corresponding to the positive value can be output by calculating the duty cycle of $V_2$ and $V_6$ separately and rounding off the negative value. That is, $V_2$ is chosen as the second voltage vector.

In summary, the proposed STV-MPCC algorithm requires optimizations only 5 times to obtain the optimal voltage vector combination.

For zero vector selection, the principle of minimum number of switching actions is followed to select between (000) and (111) switching states. For example, when the previous state output voltage of the inverter is (101), (111) is selected as the zero-vector output currently.

## 5. DUTY CYCLE MODULATION STRATEGY

The effective voltage vectors of the conventional TV-MPCC in one control cycle are selected by the cost function, and the three vectors are independent of each other, resulting in an unfixed switching frequency. Therefore, to achieve a fixed switching frequency, the selection of the second voltage vector and zero vector follows the principle of the minimum number of switching actions. In this paper, the seven-band modulation method is adopted. Compared with the five-band modulation method, only one switch state needs to be changed each time to fix the switching frequency. The timing diagram is shown in Fig. 5.

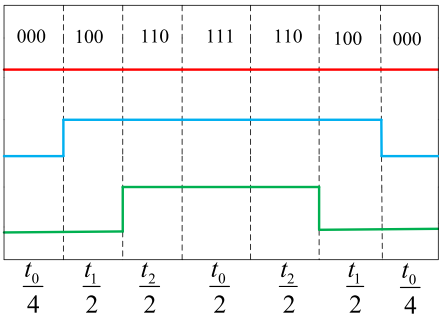


**FIGURE 5**. Timing diagram.

The current error amount is introduced in the calculation of the effective voltage action time, and the $d$-$q$ axis voltage error can be represented as

$$\begin{cases} E_d(u_i) = i_d^{ref} - i_d^{k+1}(u_i) \\ E_q(u_i) = i_q^{ref} - i_q^{k+1}(u_i) \end{cases} \tag{16}$$

where $E_d(u_i)$ and $E_q(u_i)$ are the $d$-$q$ axis voltage error, respectively; $i_d^{k+1}(u_i)$ and $i_q^{k+1}(u_i)$ are $d$-$q$ axis predicted current corresponding to the effective voltage vector, respectively, $i = 1$, 2, 3.

The output voltage is modulated using the principle of current error minimization, so that the average current error of the three voltage actions in one cycle is made to be 0, and the following expression can be obtained.

$$\begin{cases} E_d(u_1)t_1 + E_d(u_2)t_2 + E_d(u_0)t_0 = 0 \\ E_q(u_1)t_1 + E_q(u_2)t_2 + E_q(u_0)t_0 = 0 \end{cases} \tag{17}$$

where $t_0$, $t_1$, and $t_2$ denote the time of action of the zero-voltage vector and the first and second effective voltage vectors, respectively, so there are:

$$t_1 + t_2 + t_0 = T_s \tag{18}$$

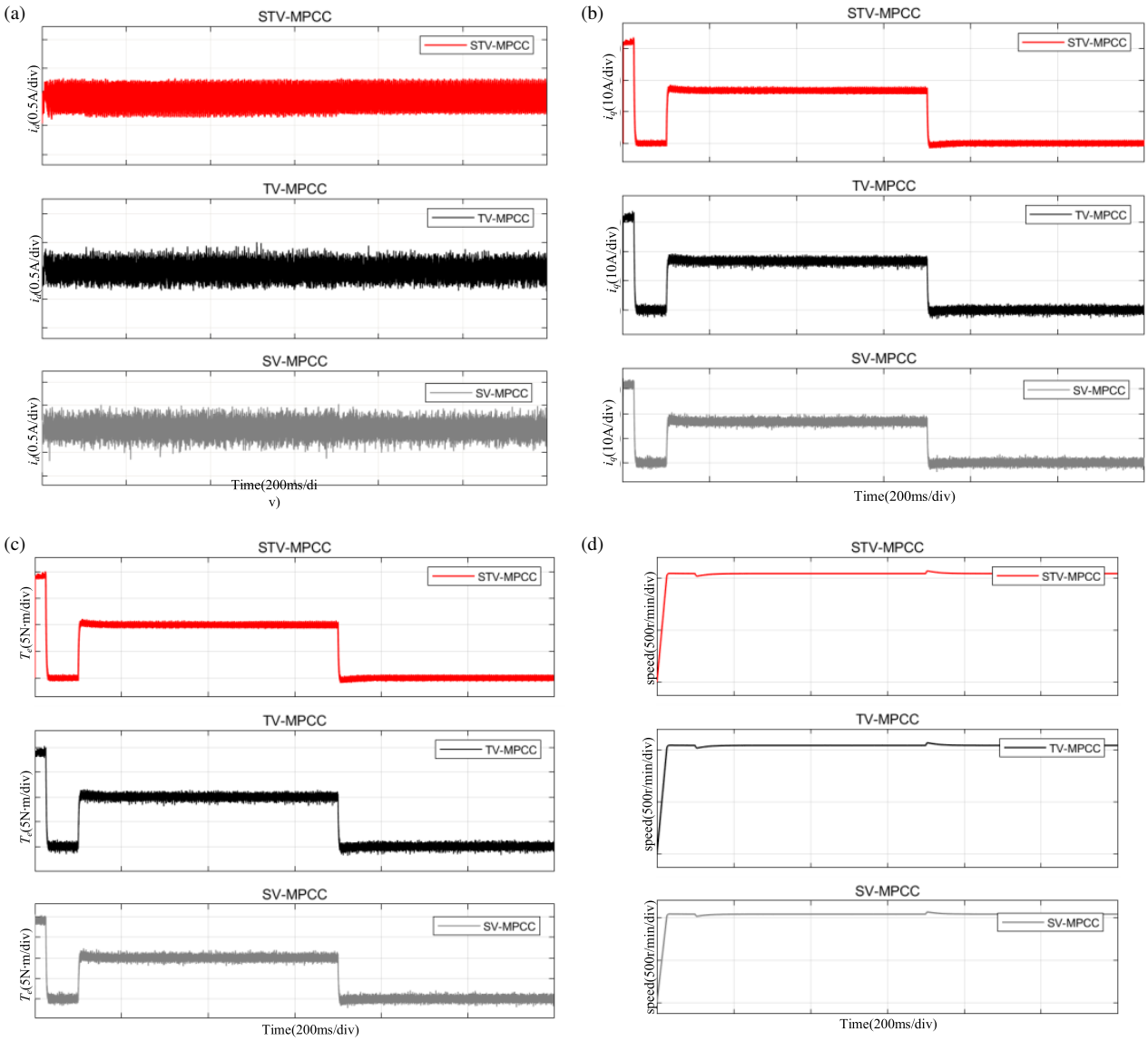


**FIGURE 6**. Simulated waveform diagram. (a) $i_d$, (b) $i_q$, (c) $T_e$, (d) $\omega_m$.

From (17) and (18), the following expression is obtained.

$$\begin{cases} t_1 = \frac{T_s}{D}\left[E_d(u_2)E_q(u_0) - E_d(u_0)E_q(u_2)\right] \\ t_2 = \frac{T_s}{D}\left[E_d(u_0)E_q(u_1) - E_d(u_1)E_q(u_0)\right] \\ t_0 = \frac{T_s}{D}\left[E_d(u_1)E_q(u_2) - E_d(u_2)E_q(u_1)\right] \end{cases} \tag{19}$$

where $D = E_d(u_0)E_q(u_1) - E_d(u_1)E_q(u_0) - E_d(u_0)E_q(u_2) + E_d(u_0)E_d(u_0) + E_d(u_2)E_q(u_0) + E_d(u_1)E_q(u_2) - E_d(u_2)E_q(u_1)$.

When the load suddenly changes, the action time may be less than zero, so it is necessary to adjust the action time.

$$\begin{cases} t_1 = \frac{T_s t_1}{t_1+t_2}\,(t_1 < 0) \\ t_2 = \frac{T_s t_2}{t_1+t_2}\,(t_2 < 0) \\ t_0 = 0(t_0 < 0) \end{cases} \tag{20}$$

The implementation steps of the STV-MPCC strategy are as follows.

1) Adopting $i_d^{ref} = 0$ control strategy, $i_q^{ref}$ is obtained by the speed loop controller, and $i_d^{k+1}$ and $i_q^{k+1}$ are calculated by (2).

2) $V_{ref}$ is calculated by (12). Select the first voltage vector through (13), (14), and (15), and select the second voltage vector from its adjacent voltage vectors.

3) The voltage vector action times $t_1$, $t_2$ and $t_3$ can be obtained by (19).

4) A seven-band modulation is used to directly output the action time to the inverter to realize the fixed switching frequency control of the motor.

## 6. EXPERIMENTAL AND SIMULATION ANALYSIS

### 6.1. Simulation Feasibility Analysis

To verify the feasibility of the proposed control method, the STV-MPCC, traditional TV-MPCC, and SV-MPCC methods are constructed using MATLAB/Simulink simulation platform. Comparative simulation analysis is conducted on the three

| Parameter | Value |
|---|---|
| Number of pole pairs | 4 |
| Stator resistance/Ω | 0.15 |
| Stator inductance/mH | 1.625 |
| Permanent magnet flux/Wb | 0.1 |
| Moment of inertia/g·cm$^2$ | 4.78 |
| Rated power/kW | 4.5 |
| Rated speed/r/min | 1000 |
| Rated torque/N·m | 10 |
| Rated voltage/V | 300 |
| Peak current/A | 32.0 |

**TABLE 1**. Parameters of PMSM.

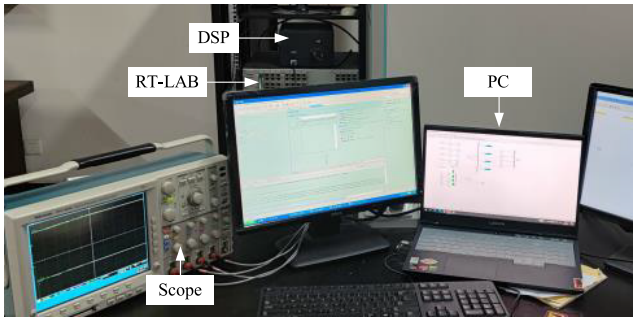


**FIGURE 7**. RT-LAB platform.

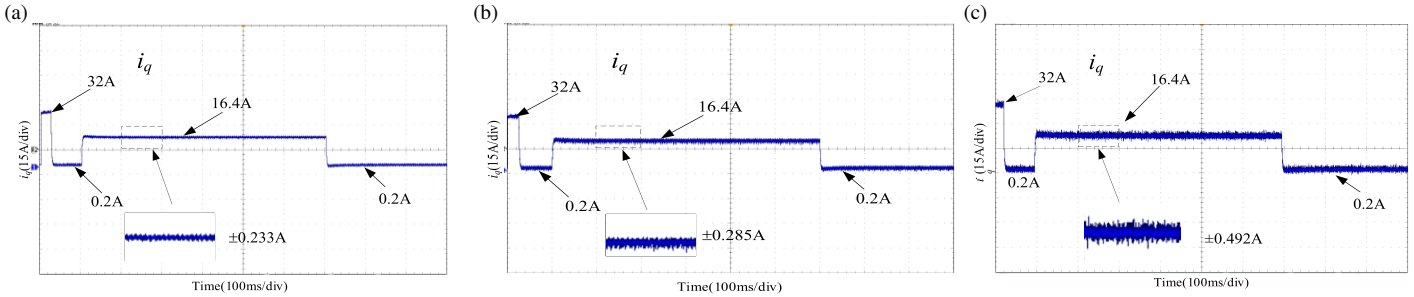


**FIGURE 8**. $q$-axis current waveform. (a) STV-MPCC, (b) TV-MPCC, (c) SV-MPCC.

methods. Fig. 7 shows the waveforms of the $d$-$q$ axis current, torque, and speed of the motor.

From Fig. 7, in terms of steady-state, compared to the TV-MPCC and SV-MPCC methods, the proposed STV-MPCC method has smoother current and torque waveforms and smaller ripple. When the load changes, the proposed STV-MPCC method demonstrates better dynamic performance.

### 6.2. Experimental Analysis

To verify the feasibility and validity of the proposed STV-MPCC strategy, the system model is built in an RT-LAB platform. The RT-LAB (OP5600) platform is shown in Fig. 6. The inverter and PMSM are constructed by RT-LAB. Both TV-MPCC and STV-MPCC strategies use the same motor parameters and discrete integral anti-saturation PI parameters ($k_i = 40$, $k_p = 2.7$), with both sampling frequencies of 20 kHz. The parameters of the PMSM are shown in Table 1.

To demonstrate the effectiveness of the proposed strategy, the proposed method is compared with the conventional TV-MPCC and SV-MPCC in a comparison experiment, and the execution times in three algorithms are recorded. The core of both TV-MPCC and STV-MPCC control strategies is to select the most suitable voltage vector, combined with the optimal duty cycle, and output to the inverter to realize the precise control of the motor. SV-MPCC selects the optimal basic effective voltage vector from six predictions within one cycle. The prediction times and average execution time of the three algorithms are shown in Table 2.

TV-MPCC requires 11 times of cost function optimization, with an average prediction time of 45.3 µs for each prediction, while the proposed STV-MPCC control strategy only requires one voltage prediction, with an average prediction time of 32.5 µs for each prediction. The calculation time is reduced by 28.2%, similar to SV-MPCC prediction time. Therefore, the proposed method effectively reduces computational complexity.

**TABLE 2**. Comparison of computational volume.

| | SV-MPCC | TV-MPCC | STV-MPCC |
|---|---|---|---|
| Number of predictions | 6 | 11 | 5 |
| Execution time (µs) | 35.4 | 45.3 | 32.5 |

To verify the steady-state and dynamic performance of the proposed method, the working conditions are set as follows: no-load start-up, 1000 r/min. The load is increased 10 N·m at 0.1 s, and unload at 0.7 s. The waveforms of $q$-axis current, electromagnetic torque, $d$-axis current, speed, and three-phase current for the three methods are shown in Figs. 7, 8, and 9.

From Fig. 8, the $i_q$ waveforms of three control strategies are smooth, and both have good steady-state characteristics. The current ripple of SV-MPCC is relatively large. Compared to TV-MPCC, STV-MPCC has less current ripple.

As can be seen in Fig. 9, in terms of steady state performance, all three control methods effectively follow the torque changes, running in steady state, and STV-MPCC has the smallest torque ripple. This is because the optional voltage vector range of the multi vector control strategy is larger, which can better suppress torque ripple. At 0.1 s, the load torque increases, and the peak torques of the three methods are 10.50 N·m, 10.55 N·m, and 10.72 N·m, respectively with an overshoot of 5%, 5.5%, 7.2%, all reaching the set torque at 0.13 s. At 0.7 s, the load torque of

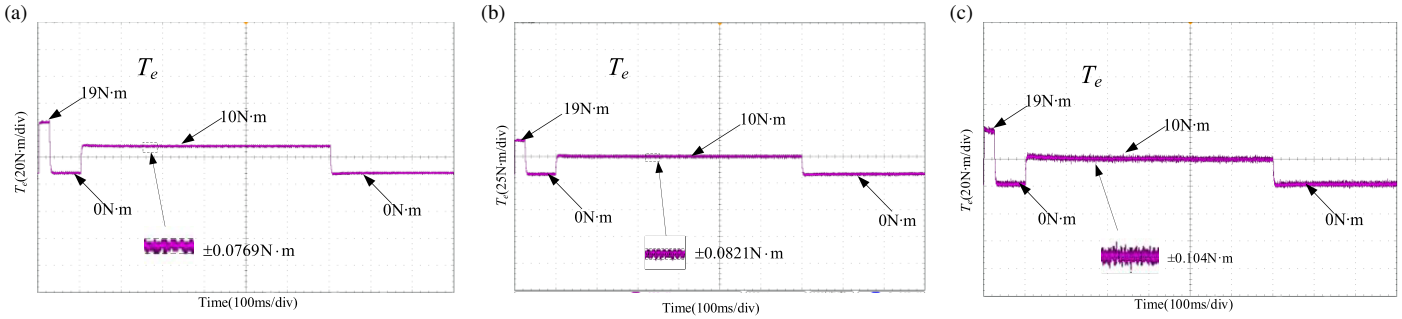


**FIGURE 9**. Electromagnetic torque waveform. (a) STV-MPCC, (b) TV-MPCC, (c) SV-MPCC.

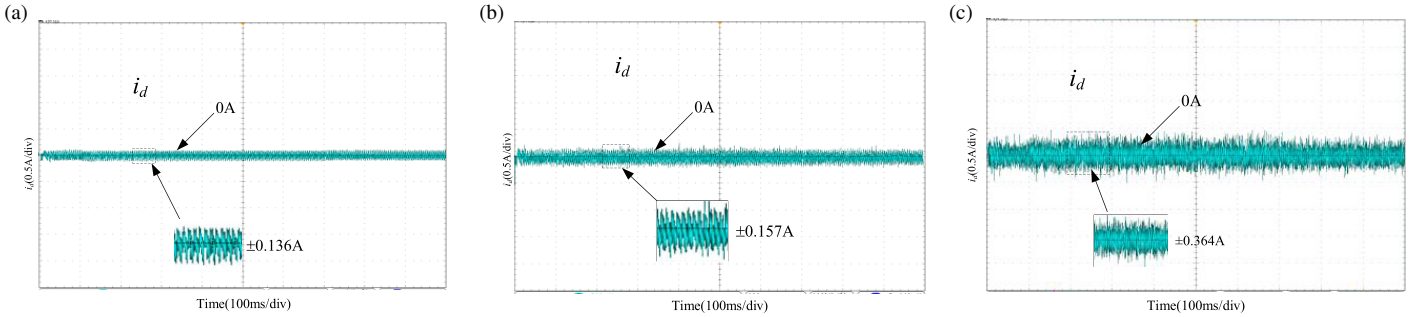


**FIGURE 10**. $d$-axis current. (a) STV-MPCC, (b) TV-MPCC, (c) SV-MPCC.

**TABLE 3**. Performance comparison.

| | operating condition | $\Delta i_d$/A | $\Delta i_q$/A | $\Delta T_e$/N·m | switching frequency |
|---|---|---|---|---|---|
| SV-MPCC | | 0.364 | 0.492 | 0.1040 | Not fixed (11.6 kHz∼20 kHz) |
| TV-MPCC | 1000 r/min, 10 N·m | 0.157 | 0.285 | 0.0821 | Not fixed (11.6 kHz∼20 kHz) |
| STV-MPCC | | 0.136 | 0.233 | 0.0769 | Fixed (11.6 kHz) |

decreases, and the minimum torque is $-0.50$ N·m, $-0.52$ N·m, $-0.66$ N·m. The torque becomes 0 at 0.73 seconds for all three methods.

As can be seen in Fig. 10, in comparison with the STV-MPCC, the $i_d$ amplitude of the TV-MPCC is reduced by 13%, with fewer burrs and a smoother waveform. The current ripple of SV-MPCC is relatively large, and its control effect is inferior to that of multi vector model predictive control.

To demonstrate that the current and torque ripple of STV-MPCC are suppressed, (21) is used to calculate the sample standard deviation of the three control strategies under the given operating conditions.

$$\begin{cases} \Delta i_d = \sqrt{\frac{1}{N}\sum_{n=1}^{N}\left(i_d\left(n\right)-i_{dave}\right)^2} \\ \Delta i_q = \sqrt{\frac{1}{N}\sum_{n=1}^{N}\left(i_q\left(n\right)-i_{qave}\right)^2} \\ \Delta T_e = \sqrt{\frac{1}{N}\sum_{n=1}^{N}\left(T_e\left(n\right)-T_{eave}\right)^2} \end{cases} \tag{21}$$

where $\Delta i_d$, $\Delta i_q$, $\Delta T_e$ are the ripple of $d$-$q$ axis current and torque. $N$ is the number of samples; $i_{dave}$, $i_{qave}$, and $T_{eave}$ are the average values of $d$-$q$ axis current and torque; $i_d(n)$, $i_q(n)$, and $T_e(n)$ are the sampled values of $d$-$q$ axis current and torque, respectively. The motor is taken at operating condition for comparison experiments. The comparison of current and torque ripple between the three strategies is shown in Table 3.

The formula for calculating the average switching frequency of three-phase inverters is

$$f = \frac{N}{12T_s} \tag{22}$$

where $N$ in the formula represents the number of switch actions within a cycle.

For a given operating condition, compared to SV-MPCC, the proposed method is superior in terms of current and torque ripple. Compared to TV-MPCC and SV-MPCC, STV-MPCC's $\Delta i_d$ are reduced by 13% and 167%; $\Delta i_q$ are reduced by 18% and 111%, respectively; and $\Delta T_e$ is reduced by 6%. Due to the fixed switching frequency of STV-MPCC, the switching loss is reduced.

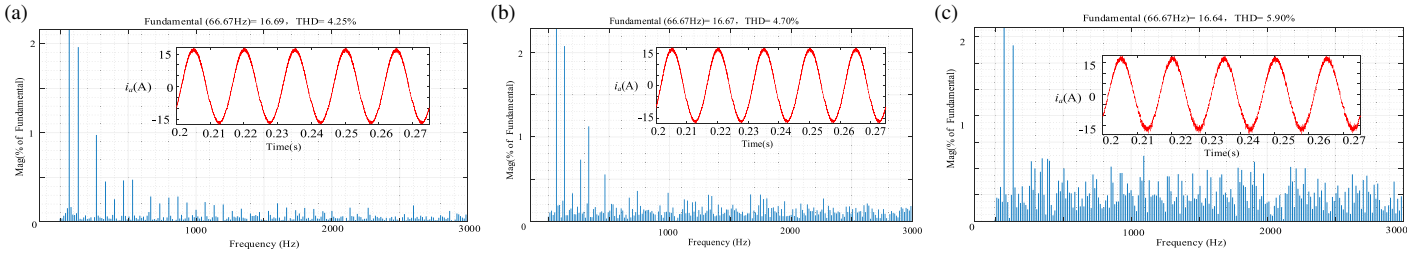


**FIGURE 11**. A-phase stator current waveform and THD analysis. (a) STV-MPCC, (b) TV-MPCC, (c) SV-MPCC.

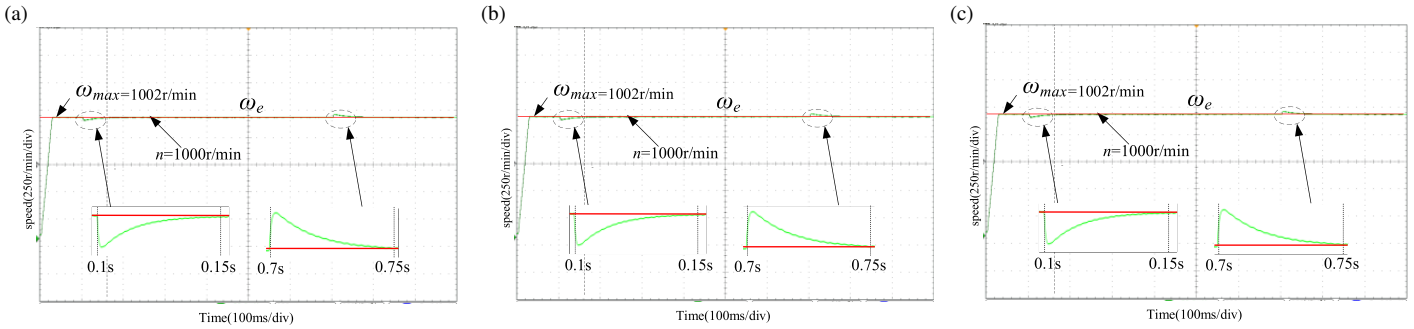


**FIGURE 12**. Motor speed. (a) STV-MPCC, (b) TV-MPCC, (c) SV-MPCC.

Figure 10 shows the A-phase stator current waveform and Total Harmonic Distortion (THD) analysis for the STV-MPCC and TV-MPCC methods. It is known that the THDs of the three methods are 4.25%, 4.70%, and 5.90%, respectively. So compared with conventional TV-MPCC and SV-MPCC, the proposed method has better steady-state performance.

In conclusion, the three-vector control method demonstrates better steady-state performance than the single-vector control method due to a much larger voltage selection range than the single-vector one. Compared with the conventional TV-MPCC method, the torque and current ripples are effectively suppressed because the proposed STV-MPCC reduces the complexity of the system and takes into account the current error in the duty cycle calculation. The calculation of (21) shows that compared to TV-MPCC, $\Delta i_d$, $\Delta i_q$, and $\Delta T_e$ of STV-MPCC are reduced by 13%, 18%, and 6%, respectively.

### 6.3. Dynamic Performance Analysis

The working conditions are set as follows: no-load start-up, 1000 r/min. The load is increased by 10 N·m at 0.1 s and unload at 0.7 s. The speed waveforms of three methods are shown in Fig. 11, respectively.

From Fig. 12, the three methods all reach the rated speed at 0.08 seconds after start-up, with an overshoot of 0.2%. At 0.10 s, the load is increased to 10 N·m, and the speed returns to the rated speed at 0.15 s. At 0.70 s unloading, the speed returned to the rated speed at 0.75 s. The results indicate that the dynamic characteristics of the three methods are consistent.

## 7. CONCLUSIONS

In this paper, a simplified three-vector selection MPCC (STV-MPCC) method for PMSM considering fixed switching frequency is proposed, which simplifies the traditional TV-MPCC algorithm and achieves the fixed switching frequency control. Through experimental verification, the following conclusions are drawn:

(1) The proposed STV-MPCC method reduces the 11 predictions of conventional TV-MPCC to 5, which decreases the computational complexity and shortens the algorithm running time.

(2) The STV-MPCC method fixes the switching frequency, reduces the switching tube losses, reduces some current harmonics. The THDs of the three methods are 4.25%, 4.70%, and 5.90%, and the energy utilization efficiency is improved.

(3) Compared with the SV-MPCC and TV-MPCC methods, the STV-MPCC method calculates the effective voltage vector action time by introducing a current error; the $q$-axis current ripple is reduced by 111% and 18%, respectively; the electromagnetic torque ripple is decreased by 35% and 6%; and the $d$-axis current burr is suppressed, which improves the dynamic performance of the system and improves the efficiency of the motor.

## ACKNOWLEDGEMENT

This work was supported by the Scientific Research Fund of Hunan Provincial Education Department under Grant Number 23B1017, Natural Science Foundation of Hunan Province of China under Grant Number 2022JJ50094.

## REFERENCES

[1] Junejo, A. K., W. Xu, C. Mu, M. M. Ismail, and Y. Liu, "Adaptive speed control of PMSM drive system based a new sliding-mode reaching law," *IEEE Transactions on Power Electronics*, Vol. 35, No. 11, 12 110–12 121, 2020.

[2] Ullah, K., J. Guzinski, and A. F. Mirza, "Critical review on robust speed control techniques for permanent magnet synchronous motor (PMSM) speed regulation," *Energies*, Vol. 15, No. 3, 1235, 2022.

[3] Orlowska-Kowalska, T., M. Wolkiewicz, P. Pietrzak, M. Skowron, P. Ewert, G. Tarchala, M. Krzysztofiak, and C. T. Kowalski, "Fault diagnosis and fault-tolerant control of PMSM drives — State of the art and future challenges," *IEEE Access*, Vol. 10, 59 979–60 024, 2022.

[4] Xu, W., A. K. Junejo, Y. Liu, M. G. Hussien, and J. Zhu, "An efficient antidisturbance sliding-mode speed control method for PMSM drive systems," *IEEE Transactions on Power Electronics*, Vol. 36, No. 6, 6879–6891, 2020.

[5] Wireko-Brobby, A., Y. Hu, G. Wang, C. Gong, W. Lang, and Z. Zhang, "Analysis of the sources of error within PMSM-based electric powertrains — A review," *IEEE Transactions on Transportation Electrification*, 2023.

[6] Candelo-Zuluaga, C., J.-R. Riba, and A. Garcia, "PMSM parameter estimation for sensorless FOC based on differential power factor," *IEEE Transactions on Instrumentation and Measurement*, Vol. 70, 1–12, 2021.

[7] Abassi, M., A. Khlaief, O. Saadaoui, A. Chaari, and M. Boussak, "Performance analysis of FOC and DTC for PMSM drives using SVPWM technique," in *2015 16th International Conference on Sciences and Techniques of Automatic Control and Computer Engineering (STA)*, 228–233, IEEE, 2015.

[8] Abu-Ali, M., F. Berkel, M. Manderla, S. Reimann, R. Kennel, and M. Abdelrahem, "Deep learning-based long-horizon MPC: Robust, high performing, and computationally efficient control for PMSM drives," *IEEE Transactions on Power Electronics*, Vol. 37, No. 10, 12 486–12 501, 2022.

[9] Sun, X., M. Wu, G. Lei, Y. Guo, and J. Zhu, "An improved model predictive current control for PMSM drives based on current track circle," *IEEE Transactions on Industrial Electronics*, Vol. 68, No. 5, 3782–3793, 2020.

[10] Xu, Y., X. Ding, J. Wang, and C. Wang, "Robust three-vector-based low-complexity model predictive current control with supertwisting-algorithm-based second-order sliding-mode observer for permanent magnet synchronous motor," *IET Power Electronics*, Vol. 12, No. 11, 2895–2903, 2019.

[11] Agoro, S. and I. Husain, "Robust deadbeat finite-set predictive current control with torque oscillation and noise reduction for PMSM drives," *IEEE Transactions on Industry Applications*, Vol. 58, No. 1, 365–374, 2021.

[12] Zhang, X., H. Bai, and M. Cheng, "Improved model predictive current control with series structure for PMSM drives," *IEEE Transactions on Industrial Electronics*, Vol. 69, No. 12, 12 437–12 446, 2021.

[13] Wu, X., M. Yang, T. Wu, K. Lu, Y. Wang, X. Liu, S. Huang, and H. Cui, "Parameter-free predictive torque and flux control for PMSM based on incremental stator flux predictive model," *IEEE Transactions on Industrial Informatics*, Vol. 20, No. 2, 2715–2726, 2024.

[14] Lan, Z., L. Jie, L. Yanhao, L. Chao, and L. Fu, "Model predictive torque control of permanent magnet synchronous motor based on fast selection table," *Transactions of China Electro Technical Society*, Vol. 38, No. 21, 5749–5757, 2023.

[15] Xu, B., Q. Jiang, W. Ji, and S. Ding, "An improved three-vector-based model predictive current control method for surface-mounted PMSM drives," *IEEE Transactions on Transportation Electrification*, Vol. 8, No. 4, 4418–4430, 2022.

[16] Dong, H. and Y. Zhang, "A low-complexity double vector model predictive current control for permanent magnet synchronous motors," *Energies*, Vol. 17, No. 1, 147, 2023.

[17] Xu, Y., J. Wang, B. Zhang, *et al.*, "Three vector model predictive current control for permanent magnet synchronous motors," *Transactions of China Electro Technical Society*, Vol. 33, No. 5, 980–988, 2018.

[18] Chen, R., H. Shu, and K. Zhai, "Three vector fixed switching frequency model predictive current control strategy for low complexity permanent magnet synchronous motors," *Proceedings of the CSEE*, 2023.

[19] Xu, Y., J. Wang, Q. Zhou, *et al.*, "Dual optimization three vector model predictive current control for permanent magnet synchronous motors," *Proceedings of the CSEE*, Vol. 38, No. 6, 1857–1864, 2018.

[20] Wen, D., Y. Zhang, and Y. Zhang, "Three-vector model-free predictive control for permanent magnet synchronous motor," *IET Power Electronics*, Vol. 16, No. 16, 2754–2768, 2023.

[21] Zhou, Q., F. Liu, and H. Gong, "Robust three-vector model predictive torque and stator flux control for PMSM drives with prediction error compensation," *Journal of Power Electronics*, Vol. 22, No. 11, 1917–1926, 2022.

[22] Duan, X., L. Kang, H. Zhou, and M. Zhao, "Three-vector model predictive power control for three-level T-type rectifier based on dead-beat control," *IET Power Electronics*, Vol. 15, No. 15, 1741–1758, 2022.

[23] Li, T., X. Sun, G. Lei, Y. Guo, Z. Yang, and J. Zhu, "Finite-control-set model predictive control of permanent magnet synchronous motor drive systems — An overview," *IEEE/CAA Journal of Automatica Sinica*, Vol. 9, No. 12, 2087–2105, 2022.